

On the Modelling of the Flow in Ducted Propellers With a Panel Method

J. Baltazar, J.A.C. Falcão de Campos

Marine Environment and Technology Center (MARETEC),
Department of Mechanical Engineering, Instituto Superior Técnico (IST), Lisbon, Portugal

ABSTRACT

This paper focus on the effect of the gap flow modelling in ducted propeller performance predictions with a panel method. Different models for the potential flow in the gap region are investigated: non-zero and zero gap width and a tip leakage model with a vortex sheet shed along the blade tip. A low order panel method for the calculation of steady potential flow on ducted propellers is used. The analysis is carried out for two configurations: propeller Ka4-70 inside duct 19A and propeller 4902 inside duct 37. The inviscid results are compared with experimental data. A strong influence of the gap model on the propeller and duct loads is found. The results indicate that the modelling of flow through the gap region is of the utmost importance for an accurate prediction of the forces on ducted propellers.

Keywords

Ducted Propeller, Panel Method, Gap Model.

1 INTRODUCTION

Ducted propeller systems are often employed to increase the efficiency and thrust of the propulsor unit in heavy loading using an accelerating type of duct or to reduce the risk of cavitation with a decelerating type of duct. Classical hydrodynamic models for describing ducted propeller systems are based on potential flow theory for an inviscid fluid. The complex interaction which occurs between propeller and duct requires some degree of simplification in the potential flow modelling. For the accelerating ducts used in practice, an accurate description of duct thickness is required and in three-dimensional flow models the simplifications mainly concerned the representation of the propeller. Kerwin et al. (1987), among others, combined a Panel Method, also known more recently as a Boundary Element Method, for the duct with a vortex lattice method for the propeller. Later such simplification has been removed, e.g. Hughes (1997) used a panel method for propeller and duct. Recently, Lee and Kinnas (2006) described a panel method for the unsteady flow analysis of ducted propeller with blade sheet cavitation. Alternative approaches to include the effective wake involved the iterative coupling of an Euler code to a lifting surface method, (Gu, 2006).

The application of inviscid flow models to ducted pro-

pellors, albeit of great usefulness, may meet some serious limitations related to the occurrence of flow regions where viscous effects can not be ignored and have to be modelled in some way. One of these regions concerns the gap flow between the propeller tip and the duct surface. Another region is the usually thick trailing edge of the duct where flow separation may ultimately determine the duct circulation.

Viscous effects may be adequately addressed by RANS calculations of the flow in a ducted propeller system. These type of calculations have already been published with considerable success in the prediction of open-water characteristics of the Wageningen Ka5 series in duct 19A at model scale, (Sanchez-Caja et al., 2000) and (Abdel-Maksoud and Heinke, 2003). A RANS-based method for the analysis of viscous flow around the duct in the presence of a propeller modelled by an actuator disk has been applied to duct 19A and the thicker duct 37 by Hoekstra (2006). The method gave predictions of duct thrust on the 19A and the velocity field around the duct 37 in good agreement with experimental data. The previous studies on the viscous flow around the duct provided valuable information on the region of flow separation close to the duct trailing edge and on important features of the flow in the gap region between propeller blades and duct. In the authors opinion, much is to be expected from RANS calculations to address the interaction between propeller and duct, especially if some coupling with the panel method may be achieved for practical design calculations.

In the potential flow model of the ducted propeller system the treatment of the gap flow and of the duct circulation remain critical issues that may drastically influence the load distribution between propeller and duct. The purpose of this paper is to focus on the effect of the gap modelling issue in the light of a limited validation study carried out for a ducted propeller in uniform flow. Different models for the potential flow in the gap region are investigated: non-zero and zero gap width and a tip leakage model with a vortex sheet shed along the chord at the tip of the propeller blade, (Gu, 2006) and (Baltazar, 2008). Other models controlling the volume flow rate through the gap and based on orifice theory have been proposed by Kerwin et al. (1987) and applied in panel methods by Hughes (1997) and Moon

et al. (2002). Nevertheless, we concentrate in this paper in the potential models as the two first models, with zero and non-zero gap width, are likely to represent the two extreme situations of propeller tip loading.

The separation from the duct trailing edge is modelled by a single vortex sheet shed from a prescribed location. For a round trailing edge the classical Kutta condition used on a sharp trailing edge is no longer applicable. A choice based on a simple geometrical criterion is used to choose the shedding location.

A low order panel method for the calculation of steady potential flow on ducted propellers is used, (Baltazar, 2008). Results are presented for two configurations: ducted propeller Ka4-70 with $P/D = 1.2$ inside duct 19A and propeller 4902 inside duct 37. For the second configuration pressure measurements carried out inside the duct in the presence of a propeller have been reported, (Falcão de Campos, 1983). The influence of the choice of the shedding line from the duct trailing edge and the influence of the gap model are first presented for the Ka4-70 ducted propeller. For the second configuration the influence of the gap model on the numerical results is investigated and compared with the pressure measurements.

2 MATHEMATICAL FORMULATION

2.1 Potential Flow Problem

Consider a propeller of radius R rotating with constant angular velocity Ω inside a duct and advancing with constant axial speed U along its axis in an incompressible ideal fluid at rest in a domain extending to infinity in all directions. The propeller is made of K blades symmetrically distributed around an axisymmetric hub. The duct is also considered to be axisymmetric and the flow field is steady in a reference frame rotating with the propeller blades. Figure 1 shows the coordinate system used to describe the propeller geometry and the fluid domain around the ducted propeller.

We introduce a Cartesian coordinate system (x, y, z) rotating with the propeller blades, with the positive x - axis direction opposite to the propeller axial motion, the y - axis coincident with the propeller reference line, passing through the reference point of the root section of the blade $k = 1$, and the z - axis completing the right-hand system. We use a cylindrical coordinate system (x, r, θ) related to the Cartesian system by

$$y = r \cos \theta, \quad z = r \sin \theta. \quad (1)$$

In the rotating frame, under the assumption of irrotational flow, the steady flow field velocity $\vec{V}(x, y, z)$ may be described by a perturbation potential $\phi(x, y, z)$ in the form

$$\vec{V} = \vec{U}_\infty + \nabla\phi, \quad (2)$$

where

$$\vec{U}_\infty = U\vec{i} + \Omega r\vec{e}_\theta \quad (3)$$

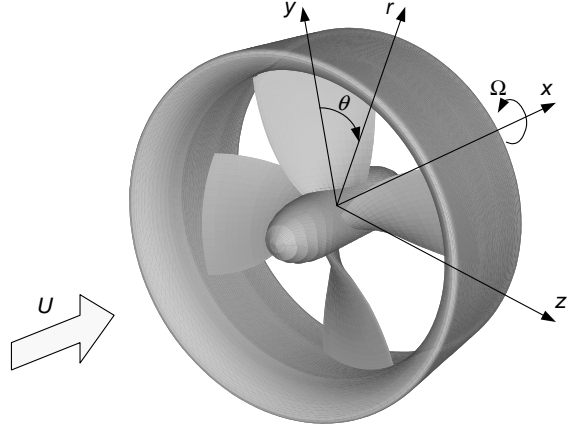


Figure 1: Propeller coordinate system.

is the undisturbed onset velocity in the rotating frame.

The perturbation potential satisfies the Laplace equation

$$\nabla^2\phi = 0. \quad (4)$$

The boundary of domain consists of the blade surfaces \mathcal{S}_B , the duct surface \mathcal{S}_D and the hub surface \mathcal{S}_H . The perturbation potential must satisfy the following boundary conditions:

$$\nabla\phi \rightarrow 0, \quad \text{if } |\vec{x}| \rightarrow \infty \quad \text{and} \quad x \neq +\infty \quad (5)$$

at infinity, and

$$\frac{\partial\phi}{\partial n} \equiv \vec{n} \cdot \nabla\phi = -\vec{n} \cdot \vec{U}_\infty \quad \text{on} \quad \mathcal{S}_B \cup \mathcal{S}_D \cup \mathcal{S}_H, \quad (6)$$

where $\partial/\partial n$ denotes differentiation along the normal and \vec{n} is the unit vector normal to the surface directed outward from the body.

To allow for the existence of circulation around the propeller blades and the duct, vortex sheets are shed from the trailing edge of the blades and the duct. The boundary conditions on the vortex sheet surfaces \mathcal{S}_W are the tangency of the fluid velocity on each side of the sheet and the continuity of the pressure across the sheet. In steady flow these conditions are

$$\frac{\partial\phi_+}{\partial n} = \frac{\partial\phi_-}{\partial n} = -\vec{n} \cdot \vec{U}_\infty, \quad p_+ = p_- \quad \text{on} \quad \mathcal{S}_W, \quad (7)$$

where p is the pressure and the indices $+$ and $-$ denote the two sides of the vortex sheets, taken, respectively, on the side of the back (normally the suction side) and face (normally the pressure side) of the blade at the trailing edge, and on the inner side and outer side of the duct at the trailing edge. In the case of the propeller blade, the unit normal to the vortex sheet is defined pointing from the face ($-$) to the back ($+$) side of the blade. In the case of the duct, the unit normal to the vortex sheet is defined pointing from the outer ($-$) to the inner ($+$) side of the duct.

In order to specify uniquely the circulation around the blades and duct it is necessary to impose the Kutta condition at the blade trailing edge and at the duct trailing edge. The Kutta condition states that the velocity must remain finite

$$|\nabla\phi| < \infty \quad (8)$$

at a sharp trailing edge.

Applying Green's second identity, assuming for the interior region to $\mathcal{S}_B \cup \mathcal{S}_D \cup \mathcal{S}_H$, $\bar{\phi} = 0$, we obtain the integral representation of the perturbation potential at a point p on the body surface,

$$2\pi\phi(p) = \iint_{\mathcal{S}_B \cup \mathcal{S}_D \cup \mathcal{S}_H} \left[G \frac{\partial\phi}{\partial n_q} - \phi(q) \frac{\partial G}{\partial n_q} \right] dS - \iint_{\mathcal{S}_W} \Delta\phi(q) \frac{\partial G}{\partial n_q} dS, \quad p \in \mathcal{S}_B \cup \mathcal{S}_D \cup \mathcal{S}_H \quad (9)$$

where $G(p, q) = -1/R(p, q)$, $R(p, q)$ is the distance between the field point p and the point q on the boundary $\mathcal{S}_B \cup \mathcal{S}_D \cup \mathcal{S}_H \cup \mathcal{S}_W$. With the $\partial\phi/\partial n_q$ on the surfaces \mathcal{S}_B , \mathcal{S}_D and \mathcal{S}_H known from the Neumann boundary condition on the body surface, Equation (6), the Equation (9) is a Fredholm integral equation of the second kind in the dipole distribution $\mu(q) = -\phi(q)$ on the surfaces \mathcal{S}_B , \mathcal{S}_D and \mathcal{S}_H . The Kutta condition, Equation (8), yields the additional relationship between the dipole strength $\Delta\phi(q)$ in the wake surfaces \mathcal{S}_W and the surface dipole strength at the blade and duct trailing edges.

2.2 Vortex Wake Model

A rigid wake model that is independent of the induced velocities is used. Contraction and pitch variation are not considered. The vortex lines shed from the blade trailing edge are assumed to lie on cylinders of constant radius. For the duct wake, a vortex sheet is shed from a prescribed location at the duct trailing edge.

2.3 Velocity, Pressure and Forces

The velocity on the surface is obtained by differentiation of the surface potential distribution. From Bernoulli's equation, the pressure coefficient C_p can be determined from

$$C_p = \frac{p - p_\infty}{1/2\rho U_\infty^2} = 1 - \left(\frac{|\vec{V}|}{U_\infty} \right)^2, \quad (10)$$

where p_∞ is the pressure of the undisturbed inflow and $|\vec{V}|$ is the total velocity.

The inviscid thrust and torque on the ducted propeller are obtained by integration of the pressure distribution on the blade and duct surfaces. The propeller operation conditions are defined by a single non-dimensional parameter: the advance coefficient $J = U/nD$, where $n = \Omega/2\pi$ is the rate of revolution and $D = 2R$ the propeller diameter. The non-dimensional thrust and torque of the ducted propeller

system are given by the propeller thrust coefficient K_{T_P} , the duct thrust coefficient K_{T_D} and the torque coefficient K_Q :

$$K_{T_P} = \frac{T_P}{\rho n^2 D^4}, K_{T_D} = \frac{T_D}{\rho n^2 D^4}, K_Q = \frac{Q}{\rho n^2 D^5}, \quad (11)$$

where T_P is the propeller thrust, T_D the duct thrust and Q the propeller torque. The total thrust coefficient of the ducted propeller is $K_{T_T} = K_{T_P} + K_{T_D}$ and the thrust ratio is

$$\tau = \frac{T_P}{T_P + T_D} = \frac{T_P}{T_T}, \quad (12)$$

which measures the contribution of the propeller thrust relative to the total thrust. The relative duct force contribution is therefore $1 - \tau$.

3 NUMERICAL METHOD

3.1 Surface Discretisation

For the numerical solution of the integral equation (9) we discretise the blade surfaces \mathcal{S}_B , the duct surface \mathcal{S}_D , the hub surface \mathcal{S}_H and the wake surfaces \mathcal{S}_W in bi-linear quadrilateral panels.

The blade is discretised in the spanwise radial direction by a number of strips, extending chordwise from the blade leading edge to the trailing edge. Cosine spacing in the radial and chordwise directions is used.

The duct surface is divided into three regions: between, upstream and downstream of the blades. The region between blades is discretised along the axial direction with the same panel spacing of the blade tip section. The regions upstream and downstream of the blades are discretised along the axial direction with a Vinokur stretching function, (Vinokur, 1983). Equidistant angular spacing is used in circumferential direction.

For the discretisation of the hub surface, an elliptical grid generator is used, (Sorensen, 1986), which requires the specification of the grid nodes on the four boundaries of the domain.

The blade and duct wake surfaces are discretised in the spanwise direction, extending downstream from the trailing edge the corresponding strips on the propeller blade and duct surfaces. A gradual variation of the panel dimensions from the trailing edge to the ultimate station far downstream is adopted.

3.2 Solution of the Integral Equation

The integral equation, Equation (9), is solved by the collocation method with the element centre point as collocation point. We assume a constant strength of the dipole and source distributions on each element. The influence coefficients are determined analytically using the formulations of Morino and Kuo (1974). To reduce the computation time, far field formulas are also used in the calculation of the influence coefficients.

The value of the dipole strength at the blade and duct trailing edges are determined by the application of a Kutta condition. The Morino Kutta condition is used as a first approximation. The condition equates the dipole strength at the trailing edge to the potential jump between the two sides of the blade and duct

$$\Delta\phi_j = \phi_j^+ - \phi_j^-, \quad (13)$$

in which ϕ_j^+ and ϕ_j^- denote the values of the potentials on the collocation points of the panels adjacent to the trailing edge on the j^{th} strip. The iterative pressure Kutta condition is applied, requiring that the pressure is equal on both sides of the blade and duct panels adjacent to the trailing edge.

3.3 Gap Flow Models

Different models for the potential flow in the gap region are considered: non-zero and zero gap width and a tip leakage model with a vortex sheet shed along the chord at the tip of the propeller blade.

In the non-zero gap model the gap is kept open and no special conditions are applied. In the zero gap width, the blade and duct grids match in the tip region. In this case, the flow is not allowed to pass between the blade tip and the duct inner surface. The blade wakes follow the duct inner surface down to the duct trailing edge.

In the tip leakage model the dipole strengths of the tip wake sheet are determined by the Morino Kutta condition, Equation (13). The pitch of the vortex line shed from the leading edge of the blade tip is assumed to be

$$\bar{P} = \frac{1}{2}(P + P_{TW}), \quad (14)$$

where P is the undisturbed flow pitch at the tip and P_{TW} is the pitch of the trailing edge wake at the blade tip. A linear variation of the pitch of the vortex lines along the chord between the leading and trailing edges is assumed. The tip leakage vortex sheet is divided into a transition wake and an ultimate wake. The ultimate region starts at $x/R = 1.0$ and has the same pitch of the trailing edge wake. In the transition wake, the pitch of the vortex lines varies along the axial direction from its value at the blade tip to the ultimate wake according to a polynomial expression, (Hoshino, 1989).

4 RESULTS

4.1 Propeller Ka4-70 Inside Duct 19A

The propeller Ka4-70 is a four-bladed propeller of the Kaplan type with a large chord at the blade tip. A pitch-diameter ratio of $P/D = 1.2$ is considered. The duct 19A has an axial cylindrical part in the inner side of the duct at the propeller location. The outer side of the duct is straight and the trailing edge of the duct is round. This duct has a length-diameter ratio of 0.5. The gap between the duct inner side and the blade tip is uniform and equal to 0.8% of the propeller radius. The particulars of the Ka-series and the duct section geometry can be found in Kuiper (1992).

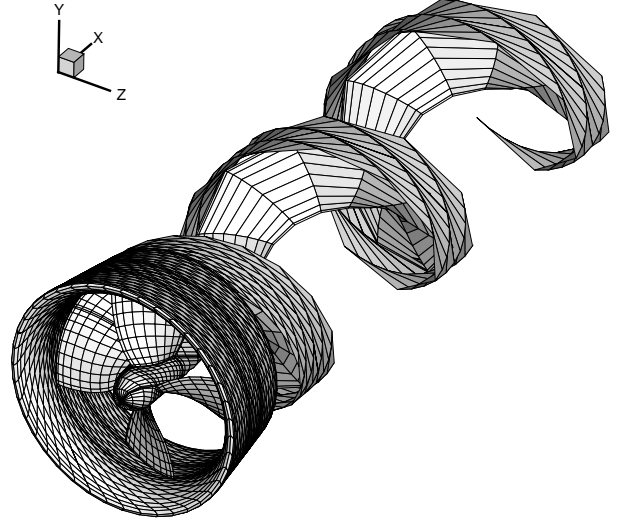


Figure 2: Panel arrangement for propeller Ka4-70 inside duct 19A. 20×11 panels on the blade; 60×10 panels on the duct sector; 21×8 panels on the hub sector; 30×10 panels on the blade and duct wakes; The length of wake is $3R$

Figure 2 shows a typical panel arrangement of propeller Ka4-70 in the duct 19A with an open-water hub. The pitch of the helicoidal wake is equal to the blade pitch.

Convergence studies of the numerical solution with the number of panels have been carried out with a non-zero gap width and are given in detail in Baltazar (2008). Convergence of the blade circulation and pressure distributions is achieved for a 40×21 blade grid, except for the pressure at close to the tip $r/R = 0.99$. The duct pressure distribution is converged for a 120×30 duct grid, except for the region close to the tip vortex. The duct circulation distribution converges more slowly.

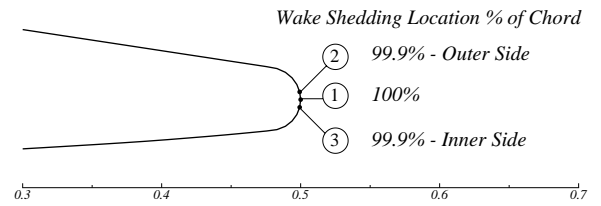


Figure 3: Location of the shedding lines for duct 19A.

The sensitivity of the calculation to the position of the wake vorticity shedding line on the duct trailing edge is investigated. Calculations were performed for the 40×21 blade grid, 120×30 duct grid and 36×16 hub grid in uniform flow at the advance coefficient $J = 0.7$. Three different locations of the shedding line are considered: at 99.9% of the duct length on the outer side and inner side of the duct, and at 100%, which is very close to the point on the "bisector" of the trailing edge angle. Figure 3 shows the trailing edge duct with the location of the wake vorticity shedding line. Figures 4 and 5 present the circulation and pressure

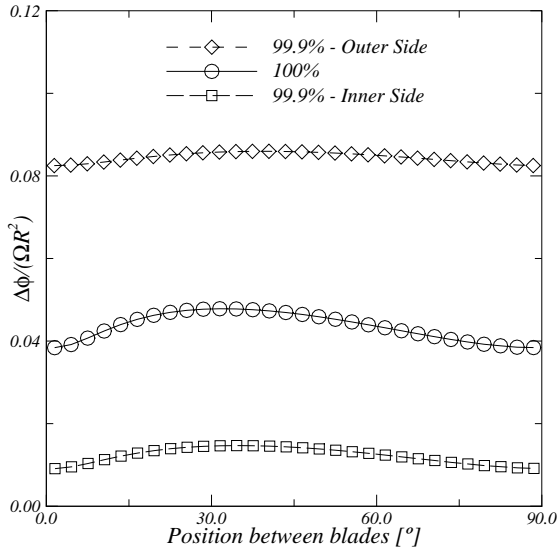
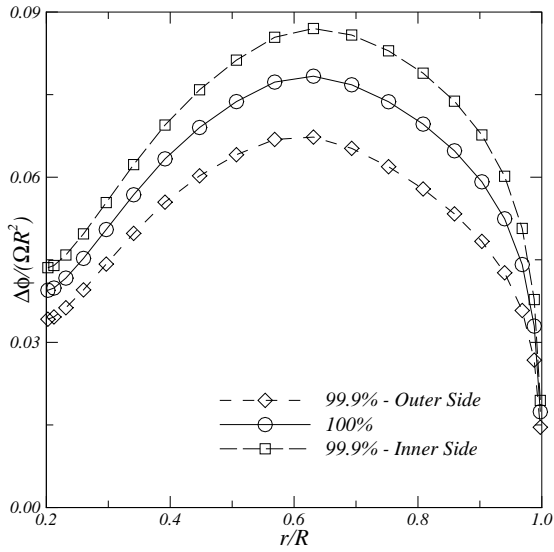


Figure 4: Blade (top) and duct (bottom) circulation distributions. Influence of the shedding line location.

distributions on the propeller blade and duct, respectively. The results show large variations in the pressure and circulation distributions with the location of the shedding line. The influence on the inviscid thrust and torque is given in Table 1. There is a considerable effect on the duct thrust. Displacing the shedding location to the outside of the round trailing edge increases the duct circulation and by inducing larger velocities on the propeller reduces the propeller loading.

The flow through the gap is considered. The relative motion between the propeller blade and duct inner side, combined with the pressure difference between the pressure and suction sides of the blade, creates a leakage flow across the tip, resulting in a strongly accelerating flow through the gap. Due to this, the flow may separate from the blade tip creating a tip leakage vortex. A detail of the vortex sheet

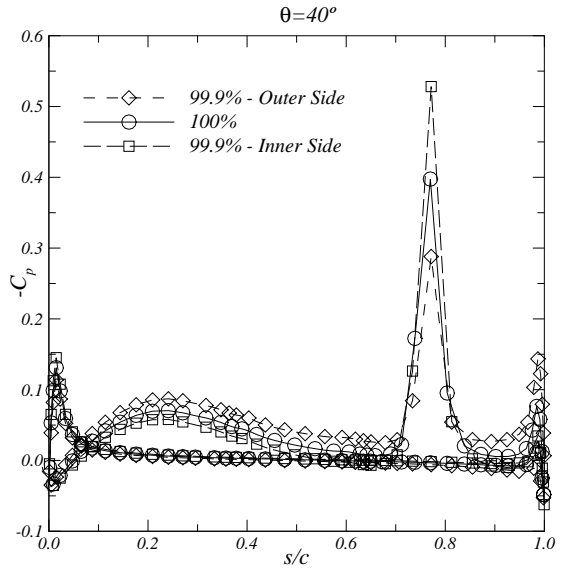
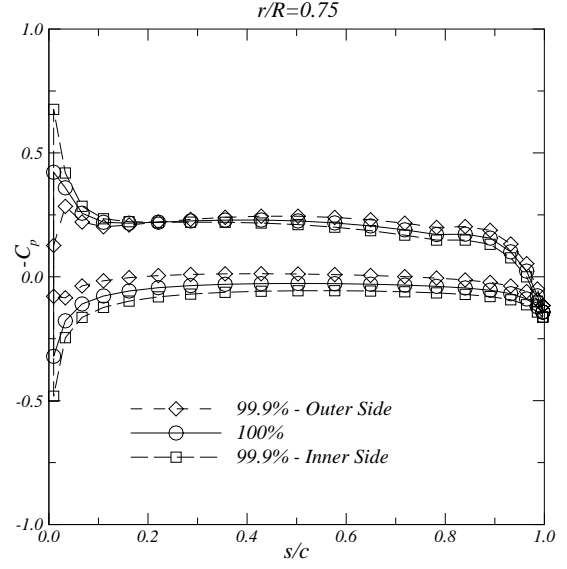


Figure 5: Blade pressure distribution at $r/R = 0.75$ (top). Duct pressure distribution at $\theta = 40$ degrees (bottom). Influence of the duct shedding line location. Ka4-70 inside duct 19A. $J = 0.7$.

Table 1: Inviscid thrust and torque coefficients on the Ka4-70 inside duct 19A. $J = 0.7$. Influence of the duct shedding line location.

Location	K_{TP}	K_{TD}	K_Q
Inner	0.3198	0.0183	0.0566
100%	0.2860	0.0287	0.0515
Outer	0.2420	0.0388	0.0447

shed from the propeller blade tip in the tip leakage model is shown in Figure 6.

Figure 7 shows the blade pressure distribution at the radial section $r/R = 0.99$ and the duct pressure distribution at the

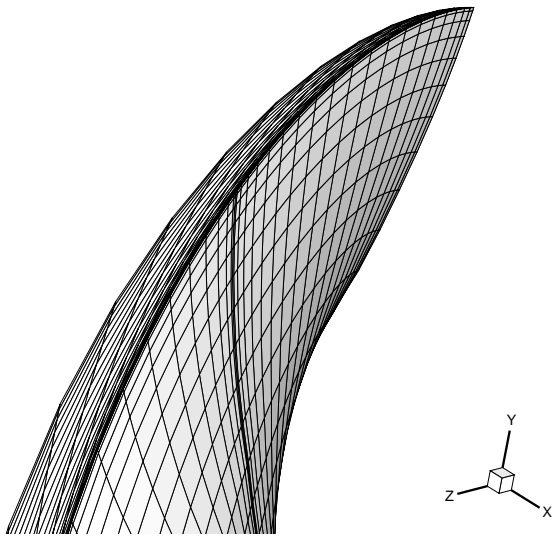


Figure 6: Detail of vortex sheet from the blade tip in the tip leakage model. Downstream view of blade pressure side.

circumferential position $\theta = 20^\circ$ with the three gap models. The blade pressure with the non-zero gap model reduces along the chordwise direction from the leading edge to the trailing edge. Such reduction is not obtained with the other gap models. For the duct pressure distribution, a suction peak is visible in the non-zero gap and tip leakage vortex models. This pressure decrease is due to the presence of the tip vortex shed from the blade trailing edge, which is close to the duct inner surface. In the tip leakage model the vorticity shed from the blade tip is distributed along the chord and reduces the suction peak. The duct pressure distribution of the zero gap width does not produce the suction peak, because the gap model does not allow vorticity to be shed from the blade tip.

Figure 8 presents the influence of the gap model on the blade and duct circulations. The blade circulation distribution tends to zero when approaching the tip in the non-zero gap model. In the zero gap model, the blade circulation at the tip is equal to the duct circulation discontinuity. Note that a finite circulation at the blade tip is also obtained in the tip leakage vortex model. In this case, the circulation distribution along the chord at the blade tip decreases from its value at the trailing edge to zero at the leading edge.

Figure 9 shows the comparison of the thrust and torque coefficients with experimental data from open-water diagrams, (Kuiper, 1992). The non-zero gap and tip leakage vortex models tend to over-predict the total thrust and torque coefficients and under-predict the duct thrust. The zero-gap model allows more loading to be transferred to the duct and is likely to overpredict the duct thrust. Note, however that no viscous corrections have been included.

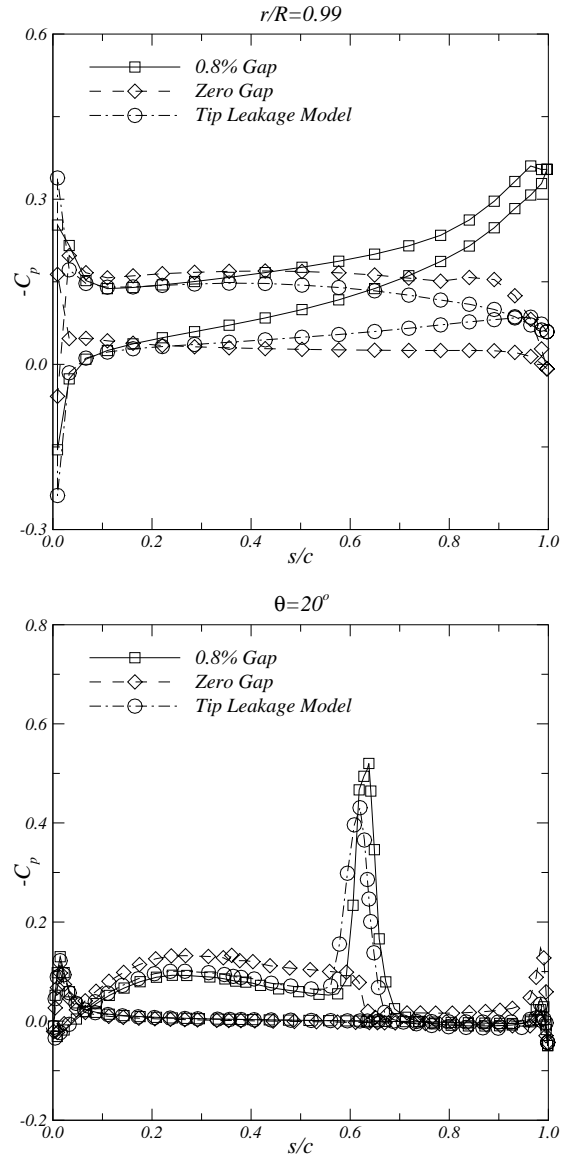


Figure 7: Influence of the gap model on the blade pressure distribution at section $r/R = 0.99$ (top) and on the duct pressure pressure distribution at $\theta = 20^\circ$ (bottom). Ka4-70 inside duct 19A. $J = 0.7$.

4.2 Pressure Distribution Inside Duct 37 with Propeller 4902

The propeller 4902 is a four-bladed controllable pitch propeller of Kaplan type with round blade tip. The duct 37 has a length-diameter ratio of 0.5 and a blunt trailing edge, (Kuiper, 1992). The gap between the duct inner side and the blade tip is uniform and equal to 0.7% of the propeller radius. The geometry of the ducted propeller is given in Falcão de Campos (1983). Calculations were performed for the 40×21 blade grid, 120×30 duct grid and 52×16 hub grid with the three gap models at the advance coefficients $J = 0.203$, $J = 0.406$ and $J = 0.617$. The helical vortex wake has the same pitch of the propeller blades. The duct vortex shedding line is at the extreme point of the duct

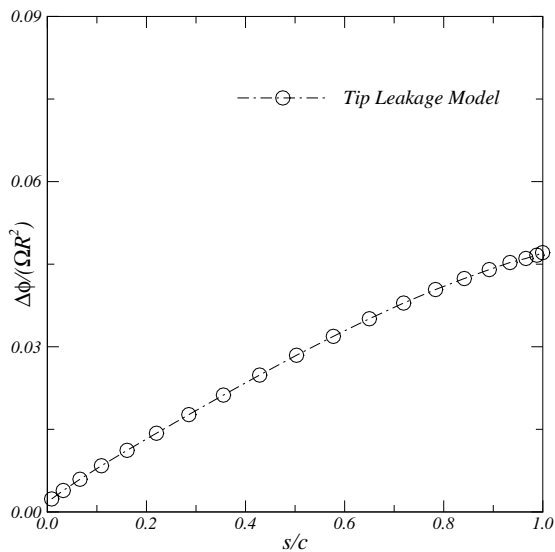
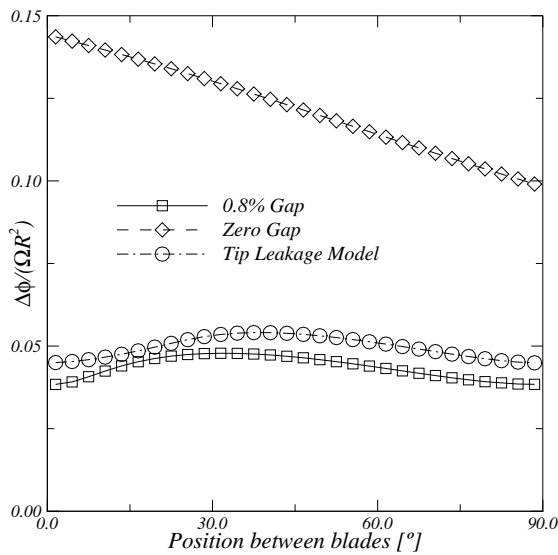
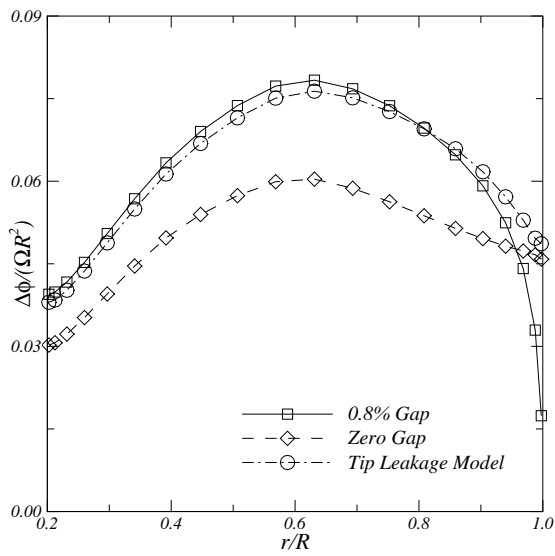


Figure 8: Influence of the gap model on the circulation distributions: blade circulation (top), duct circulation (middle) and blade tip circulation (bottom). Ka4-70 inside duct 19A

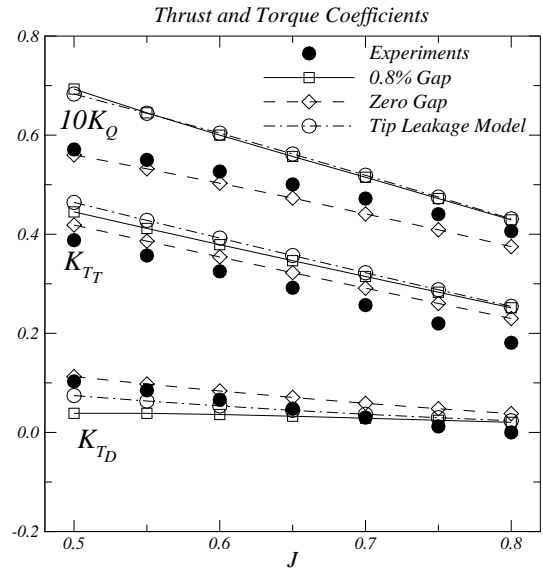


Figure 9: Inviscid thrust and torque coefficients. Comparison with open-water data. Ka4-70 inside duct 19A, $P/D = 1.0$

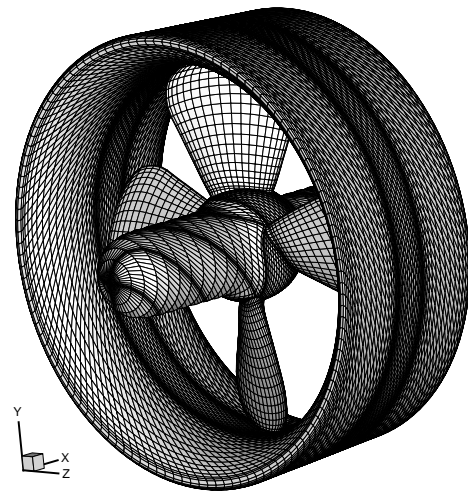


Figure 10: Panel arrangement for propeller 4902 inside duct 37.

length in all cases. The panel arrangement used for the calculations is illustrated in Figure 10.

A set of experiments with the propeller 4902 inside the duct 37 has been carried out at MARIN (Maritime Research Institute Netherlands) in the Netherlands. The unsteady pressure distribution on the inner side of the duct at different propeller loadings was measured in the depressurised towing tank (in atmospheric condition). The zeroth harmonic is reported in (Falcão de Campos, 1983). Figure 11 shows the pressure distribution over the duct surface calculated with the three gap models. There is a remarkable difference between the models. None of the models seem to predict correctly the shape of the pressure distribution. The zero-gap model is closest to the experimental pressure in front of

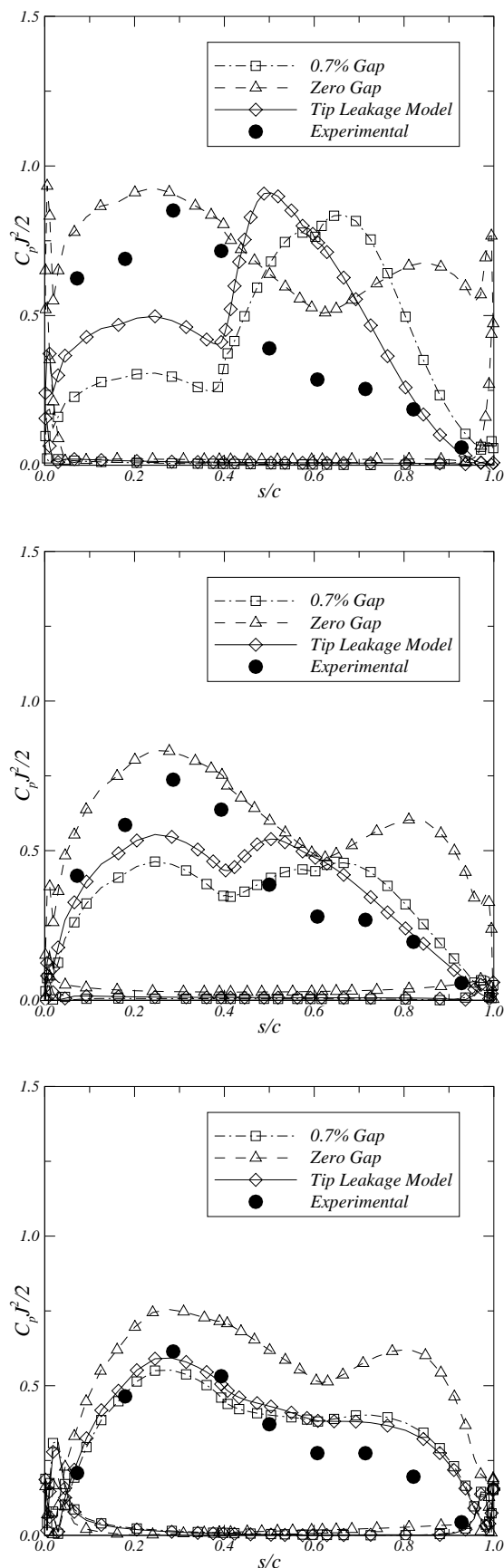


Figure 11: Influence of the gap model on the mean pressure distribution: $J = 0.203$ (top), $J = 0.405$ (middle) and $J = 0.617$ (bottom). Propeller 4902 inside duct 37.

the propeller at low advance ratios but introduces too high loadings downstream of the propeller. Note that in this case the blade wakes expand following the duct inner surface. The non-zero gap and the tip leakage model show unrealistic pressure peaks due to the presence of strong vorticity shed from the propeller blade tip and are not able to sustain the blade loading at the tip which unloads the duct. At the highest advance ratio this effect is less evident. We note that part of the discrepancies may be due to lack of proper propeller wake alignment inside the duct. This should be investigated further.

5 CONCLUDING REMARKS

A low order panel method has been used to analyse the flow around the Ka4-70 ducted propeller with duct 19A in uniform flow. The predictions of the duct and propeller loading were found to be critically dependent on the gap model. Also the location of the duct vortex sheet shedding line is found to have a strong influence on the results. The non-zero gap model and the tip leakage model produce considerably lower duct loadings than the zero-gap model. For the propeller 4902 inside the duct 37 none of the gap models was able to predict the shape of the pressure distribution inside the duct. The non-zero gap model and the tip leakage model produce unrealistic pressure distributions on the duct in the vicinity of the propeller. The zero-gap model predicts too high loadings in the downstream part of the duct.

It is suggested that the influence of wake alignment should be investigated for the case of a duct with a sharp trailing edge to avoid the uncertainty in the duct wake. In addition, a more realistic tip leakage model in combination with the orifice model could be investigated.

6 ACKNOWLEDGMENTS

The first author acknowledges the financial support granted by Fundação para a Ciência e a Tecnologia, Ph.D. grant SFRH/BD/14334/2003.

REFERENCES

- Abdel-Maksoud, M. and Heinke, H.-J. (2003). ‘Scale effects on ducted propellers’. In *Twenty-Fourth Symposium on Naval Hydrodynamics*, Fukuoka, Japan.
- Baltazar, J. (2008). *On the Modelling of the Potential Flow About Wings and Marine Propellers Using a Boundary Element Method*. PhD Thesis, Instituto Superior Técnico, Technical University of Lisbon.
- Falcão de Campos, J. A. C. (1983). *On the Calculation of Ducted Propeller Performance in Axisymmetric Flows*. PhD Thesis, Delft University of Technology.
- Gu, H. (2006). *Numerical Modeling of Flow Around Ducted Propellers*. PhD Thesis, The University of Texas at Austin.

- Hoekstra, M. (2006). 'A RANS-based analysis tool for ducted propeller systems in open water condition'. International Shipbuilding Progress, 53:205 – 227.
- Hoshino, T. (1989). 'Hydrodynamic analysis of propellers in steady flow using a surface panel method. 2nd report: Flow field around propeller'. Journal of The Society of Naval Architects of Japan, 166:79 – 92.
- Hughes, M. J. (1997). 'Implementation of a special procedure for modeling the tip clearance flow in a panel method for ducted propellers'. In Propellers/Shafting '97 Symposium, Virginia Beach, USA.
- Kerwin, J. E., Kinnas, S. A., Lee, J.-T., and Shih, W.-Z. (1987). 'A surface panel method for the hydrodynamic analysis of ducted propellers'. In Transactions of Society of Naval Architects and Marine Engineers, volume 95, Teddington, England.
- Kuiper, G. (1992). The Wageningen Propeller Series. MARIN Publication 92-001.
- Lee, H. and Kinnas, S. A. (2006). 'Prediction of cavitating performance of ducted propellers'. In Sixth International Symposium on Cavitation, Wageningen, The Netherlands.
- Moon, I.-S., Kim, K.-S., and Lee, C.-S. (2002). 'Blade tip gap flow model for performance analysis of waterjet propulsors'. In International Association for Boundary Element Methods, Austin, Texas, USA.
- Morino, L. and Kuo, C.-C. (1974). 'Subsonic potential aerodynamics for complex configurations: A general theory'. AIAA Journal, 12(2):191 – 197.
- Sanchez-Caja, A., Rautahaimo, P., and Siikonen, T. (2000). 'Simulation of incompressible viscous flow around a ducted propeller using a rans equation solver'. In Twenty-Third Symposium on Naval Hydrodynamics, Val de Reuil, France.
- Sorensen, R. L. (1986). 'Three-dimensional elliptic grid generation about fighter aircraft for zonal finite-difference computations'. In AIAA-86-0429. AIAA 24th Aerospace Sciences Conference, Reno, NV.
- Vinokur, M. (1983). 'On one-dimensional stretching functions for finite-difference calculations'. Journal of Computational Physics, 50:215 – 234.